Computational Mechanics 20 (1997) 427 – 438 © Springer-Verlag 1997

Finite dynamic deformations of smart structures

R. C. Batra, X. Q. Liang

Abstract We study transient finite deformations of a neoHookean beam or plate with piezoelectric (PZT) patches bonded to its upper and lower surfaces. The constitutive relations for the PZTs are taken to be linear in the Green-Lagrange strain tensor but quadratic in the driving voltage. A finite element code using 8-noded brick elements has been developed and validated by comparing computed results with either analytical solutions or experimental observations. For flexural waves propagating through a cantilever beam, the sensor output is influenced a little by the presence of a defect placed symmetrically about the centroidal axis. A simple feedback control algorithm is shown to control the motion of a neoHookean plate subjected to an impulsive load.

1 Introduction

Smart structural elements usually consist of a composite substrate and piezoelectric (PZT) patches either bonded to the substrate's outer surfaces or embedded in the structure. They generally can sense and control their undesired vibrations. They are used to control vibrations of space structures (e.g. see Hall and Muller 1995; Dosch et al. 1993; Won et al. 1994), improve acoustics (e.g. see Johnson and Elliot 1995; Price and Napoletano 1995; Fuller et al. 1991), and suppress the flutter of aircraft panels (e.g. see Heeg et al. 1995; Song et al. 1992). Because of the difficulty in accurately modeling the interaction between PZTs and the substrate, analytical solutions of smart structure problems are limited to their infinitesimal deformations and simple geometries (e.g. see Ray et al. 1993; Lagoudas and Bo 1994; Brooks and Heyliger 1994; Srinivas et al. 1970; Wittrick 1987; Zhou and Tiersten 1994; Batra and Liang 1996). Numerous authors have used the finite element method (FEM) to analyse smart structural problems by using either a beam theory (e.g. see Hanagud et al. 1987; Im and Atluri 1989; amongst others), a plate theory (Chandrashekhara and Agarwal 1993; Batra and Ghosh 1995; Samanta et al. 1996; Suleman and Venkayya 1995; amongst others), and a shell theory (Tzou and Gadre 1989; Qiu and Tami 1996; amongst others). The three-dimensional FEM has been used by Allik and Hughes (1970), Mollenhauer and Griffin (1994), Tzou et al. (1994), Hauch (1995) and others. Wojicik et al. (1993) have argued that the explicit algorithm is more appropriate for studying the transient response of large smart structures.

Whereas foregoing studies have considered infinitesimal deformations and hence have used linear material models, Norwood et al. (1991), Kulkarni and Hanagud (1991), and Pai et al. (1992) have accounted for material and/or geometric nonlinearities. Crawley and Anderson (1990) experimentally showed that the normal strain vs. electric field relation for the G1195 PZT is highly nonlinear for driving electric fields exceeding 100 V/mm. Tiersten (1993) has successfully modeled these experiments by using a theory linear in displacement gradients but cubic in the electric field. Maugin et al. (1992) and Tiersten (1971, 1975) have developed fully nonlinear material models that account for both finite deformations and large electric fields. Yang and Batra (1995) have derived second-order form invariant polynomial constitutive relations for transversely isotropic and orthotropic PZTs. Huang and Batra (1996) have generalized these to include heat conduction and viscous effects.

Here we analyse three-dimensional nonlinear smart structure problems by the FEM and model the substrate and the PZT by second-order form invariant polynomial constitutive relations. The problem formulation accounts for the bending and stretching deformations of the PZTs and the substrate. Because of the difficulty in ascertaining values of material parameters, results are presented for a neo-Hookean substrate and the PZT modeled by a constitutive relation linear in the Green-Lagrange strain tensor but quadratic in the electric field. Both Crawley and Anderson's experiments on a PZT plate and Moetakef et al.'s (1996) experiments on flexural waves in an aluminum beam generated by PZT patches bonded near its free end are simulated. Computed results are found to be in general agreement with the test observations. The transverse velocity of a point on the surface of a neoHookean cantilever beam is not affected much by the presence of a narrow defect near its centroidal axis. A simple feedback algorithm is shown to control well the vibrations of a cantilever smart plate.

Communicated by S. N. Atluri, 12 March 1997

R. C. Batra, X. Q. Liang
Department of Engineering Science and Mechanics,
Virginia Polytechnic Institute and State University,
Blacksburg, VA 24061-0219, USA

Correspondence to: R. C. Batra

This work was supported by the NSF grant CMS9713453 to Virginia Polytechnic Institute and State University, and the U.S. Army Research Office grant DAAH04-93-G-0214 to the University of Missouri-Rolla, and a matching grant from the Missouri Research and Training Center. Virginia Polytechnic Institute and State University acted as a subcontractor.

2 Formulation of the problem

Consider a smart structure occupying the region Ω in the reference configuration with region Ω_s occupied by a substrate and Ω_p by a piezoelectric material bonded perfectly to the substrate at their common interface $\partial\Omega_{\text{int}} = \partial\overline{\Omega}_s \cap \partial\overline{\Omega}_p$. Using rectangular Cartesian coordinates and the referential description of motion, equations governing finite deformations of the structure are

$$T_{Li,L} + \rho_0 b_i = \delta_{iM}\rho_0 \ddot{u}_M \quad \text{in} \quad \Omega \tag{1}$$

$$D_{L,L} = 0 \qquad \text{in} \quad \Omega_p \ . \tag{2}$$

Here T_{Li} is the first Piola-Kirchhoff stress tensor, upper case indices refer to Cartesian coordinates $\mathbf{X}$ in the reference configuration and lower case indices to those ($\mathbf{x}$) in the present configuration, a comma followed by an index $L(i)$ implies partial differentiation with respect to $X_L(x_i)$, a repeated index implies summation over the range of the index, δ_{iM} is the Kronecker delta, $\mathbf{b}$ the present body force per unit mass, ρ_0 the mass density, $\mathbf{u}$ the displacement of a point, a superimposed dot indicates the material time derivative, and $\mathbf{D}$ is the electric displacement. Because of small permittivity of the free space, the Maxwell electrostatic stress tensor has been neglected. We have also neglected the effect of body charges and inertia associated with the electric displacement field. The pertinent boundary conditions are

$$\mathbf{u} = \hat{\mathbf{u}} \quad \text{on} \quad \partial\Omega_u \ , \tag{3.1}$$

$$T_{Li}N_L = \hat{f}_i \quad \text{on} \quad \partial\Omega_t \ , \tag{3.2}$$

$$\phi = \hat{\phi} \quad \text{on} \quad \partial\Omega_\phi \ , \tag{3.3}$$

$$D_L N_L = \hat{D} \quad \text{on} \quad \partial\Omega_e \ , \tag{3.4}$$

$$[\mathbf{u}] = 0,\ [T_{Li}]N_L = 0 \quad \text{on} \quad \partial\Omega_{\text{int}} \ . \tag{3.5}$$

That is displacements are prescribed as $\hat{\mathbf{u}}$ on $\partial\Omega_u$, surface tractions as $\hat{\mathbf{f}}$ on $\partial\Omega_t$, the electric potential as $\hat{\phi}$ on $\partial\Omega_\phi$, and the normal component of electric displacement as $\hat{D}$ on $\partial\Omega_e$. Here N is an outward unit normal to $\partial\Omega$. In Eq. (3.5), $[\mathbf{u}] = \mathbf{u}^P - \mathbf{u}^S$ where $\mathbf{u}^P(\mathbf{u}^S)$ denotes the displacements of a piezoelectric (substrate) point on $\partial\Omega_{\text{int}}$. Equations (3.5) imply that displacements and surface tractions are continuous across $\partial\Omega_{\text{int}}$ which is equivalent to the assumption that the piezoelectric material and the substrate are perfectly bonded to each other. The electric displacement $\mathbf{D}$ is related to the electric potential ϕ through

$$D_L = P_L + \epsilon_0 J X_{L,i} X_{K,i} W_K \ , \tag{4.1}$$

$$W_L = -\phi_{,L} \ , \tag{4.2}$$

where $\mathbf{P}$ is the electric polarization vector, ϵ_0 the permittivity of the free space, $J = \det(F_{iL})$, $F_{iL} = x_{i,L}$, $\mathbf{W}$ is the material electric field, and ϕ the electric potential.

We assume that the piezoelectric material is transversely isotropic. Because of the difficulty in determining from the scant experimental data explicit expressions for the response functions of a nonlinear transversely isotropic piezoelectric material, we employ a second-order theory for it. With unit vector $\mathbf{a}$ pointing in the direction of transverse isotropy and assuming that the piezoelectric plate is initially stress free, we postulate the following (Yang and Batra 1995).

$$\begin{aligned}
\overline{\mathbf{T}} \ = \ & (2c_1 I_1 + c_3 I_2 + e_1 I_3 + 3\lambda_1 I_1^2 + 2\lambda_3 I_1 I_2 + \lambda_4 I_2^2 + \lambda_5 II_1 \\
& + \lambda_7 II_2 + 2\nu_1 I_1 I_3 + \nu_2 I_3^2 + \nu_7 II_3 + \nu_9 II_4 \\
& + \nu_{14} I_2 I_3)\mathbf{a}\otimes\mathbf{a} + (2c_2 I_2 + c_3 I_1 + e_2 I_3 + 3\lambda_2 I_2^2 \\
& + \lambda_3 I_1^2 + 2\lambda_4 I_1 I_2 + \lambda_6 II_1 + \lambda_8 II_2 + 2\nu_3 I_2 I_3 \\
& + \nu_4 I_3^2 + \nu_8 II_3 + \nu_{10} II_4 + \nu_{14} I_1 I_3)\mathbf{1} \\
& + (c_4 + \lambda_5 I_1 + \lambda_6 I_2 + \nu_5 I_3)(\mathbf{a}\otimes\mathbf{E}\cdot\mathbf{a} + \mathbf{a}\cdot\mathbf{E}\otimes\mathbf{a}) \\
& + 2(c_5 + \lambda_7 I_1 + \lambda_8 I_2 + \nu_8 I_3)\mathbf{E} \\
& + (e_3 + \nu_9 I_1 + \nu_{10} I_2 + \nu_{11} I_3)(\mathbf{a}\otimes\mathbf{W} + \mathbf{W}\otimes\mathbf{a}) \\
& + 3\lambda_9 \mathbf{E}^2 + \nu_{12}\mathbf{W}\otimes\mathbf{W} + \nu_{13}(\mathbf{a}\otimes\mathbf{E}\cdot\mathbf{W} + \mathbf{W}\cdot\mathbf{E}\otimes\mathbf{a} \\
& + \mathbf{W}\otimes\mathbf{E}\cdot\mathbf{a} + \mathbf{a}\cdot\mathbf{E}\otimes\mathbf{W}) \ ,
\end{aligned} \tag{5}$$

$$\begin{aligned}
-\mathbf{P} \ = \ & (2\epsilon_1 I_3 + e_1 I_1 + e_2 I_2 + 3\mu_1 I_3^2 + \mu_2 II_3 + \nu_1 I_1^2 \\
& + 2\nu_2 I_3 I_1 + \nu_3 I_2^2 \\
& + 2\nu_4 I_3 I_2 + \nu_5 II_1 + \nu_6 II_2 + \nu_{11} II_4 + \nu_{14} I_1 I_2)\mathbf{a} \\
& + 2(\epsilon_2 + \mu_2 I_3 + \nu_7 I_1 + \nu_8 I_2)\mathbf{W} \\
& + 2(e_3 + \nu_9 I_1 + \nu_{10} I_2 + \nu_{11} I_3)\mathbf{E}\cdot\mathbf{a} \\
& + 2\nu_{12}\mathbf{E}\cdot\mathbf{W} + 2\nu_{13}\mathbf{E}^2\cdot\mathbf{a} \ .
\end{aligned} \tag{6}$$

Here $\overline{\mathbf{T}}$ is the second Piola-Kirchhoff stress tensor, $\mathbf{E}$ the Green-Lagrange strain tensor, $c_1, c_2 \ldots, c_5$, $\lambda_1, \ldots, \lambda_8$, $\nu_1, \ldots, \nu_{14}$, e_1, e_2, e_3, ϵ_1, ϵ_2, μ_1 and μ_2 are material constants, and

$$\begin{aligned}
& I_1 = \mathbf{a}\cdot\mathbf{E}\mathbf{a}, \quad I_2 = \text{tr } \mathbf{E}, \quad I_3 = \mathbf{a}\cdot\mathbf{W}, \quad II_1 = \mathbf{a}\cdot\mathbf{E}^2\mathbf{a}, \\
& II_2 = \text{tr } \mathbf{E}^2, \quad II_3 = \mathbf{W}\cdot\mathbf{W}, \quad II_4 = \mathbf{a}\cdot\mathbf{E}\mathbf{W} + \mathbf{W}\cdot\mathbf{E}\mathbf{a} \ ,
\end{aligned} \tag{7}$$

and $\mathbf{u}\otimes\mathbf{v}$ denotes the tensor product between vectors $\mathbf{u}$ and $\mathbf{v}$. The neo-Hookean model follows from Eqs. (5) and (6) by keeping only terms linear in $\mathbf{E}$ and $\mathbf{W}$, the small deformation/large driving voltage theory of Tiersten (1993) follows from Eqs. (5) and (6) when $\mathbf{E}$ is replaced by the infinitesimal strain tensor, and the conventional linear piezo-electric constitutive relations are obtained by keeping only terms linear in $\mathbf{W}$ and the displacement gradients; these equations have been derived by Yang and Batra (1995). The second-order constitutive relation for a transversely isotropic substrate follows from Eq. (5) by setting $\mathbf{W} = 0$, and that for a neo-Hookean transversely isotropic substrate by keeping terms linear in $\mathbf{E}$. For an orthotropic neo-Hookean substrate

$$\overline{\mathbf{T}} = \mathbf{C}\mathbf{E} \tag{8}$$

where the fourth order elasticity tensor $\mathbf{C}$ has the same form as the one in linear elasticity.

The Green-Lagrange strain tensor is related to displacements $\mathbf{u}$ through

$$E_{KL} = (u_{K,L} + u_{L,K} + u_{M,K}u_{M,L})/2 \ , \tag{9}$$

and the first and the second Piola-Kirchhoff stress tensors are related as

$$T_{Ki} = x_{i,L}\overline{T}_{KL} \ . \tag{10}$$

The Cauchy stress tensor σ_{ij} can be computed from $\overline{T}_{KL}$ by using

$$\sigma_{ij} = J^{-1}x_{i,K}x_{j,L}\overline{T}_{KL} \ . \tag{11}$$

In order to complete the formulation of the problem, we need to specify initial displacements and initial velocities; we take these to be zero.

3
Finite element formulation

Following Hughes (1987) the weak formulation of Eqs. (1) and (2) can be written as

$$\delta_{iM}\delta_{iN}\int_\Omega \rho\ddot{u}_M v_N \mathrm{d}\Omega = \delta_{iN}\left[\int_{\partial\Omega_t}\hat{f}_i v_N \mathrm{d}S - \int_\Omega T_{Li}v_{N,L}\mathrm{d}\Omega\right] \ , \tag{12a}$$

$$\int_\Omega D_L\psi_{,L}\mathrm{d}\Omega = \int_{\partial\Omega_e}\hat{D}\psi \mathrm{d}S \ , \tag{12b}$$

where v_N is a virtual displacement vector that vanishes on $\partial\Omega_u$ and ψ is a virtual electric potential that vanishes on $\partial\Omega_\phi$. The left-hand side of Eq. (12a) equals the virtual work of inertia forces, the first term on its right-hand side represents the virtual work of externally applied tractions, and the second term equals the virtual work done by internal stresses. Note that internal stresses depend upon the mechanical deformation and the electric charge in piezoelectric materials. The left-hand side of Eq. (12b) equals the virtual internal electric energy, and the right-hand side is the virtual electric energy due to surface charge on the piezoelectric material. Substitution for T_{Li} from (5) and (10), and for D_L from (4.1), (4.2) and (6) yields equations for the determination of displacements $\mathbf{u}$ and the electric potential ϕ. We discretize the domain Ω into the union of 8-noded brick elements and employ a $2\times2\times2$ quadrature rule to numerically evaluate various integrals over an element. Referring the reader to Hughes (1987) for details, we note that Eqs. (12) yield the following set of coupled nonlinear ordinary differential-algebraic equations.

$$\mathbf{M}\ddot{\mathbf{d}} = \mathbf{F}^{\mathrm{ext}}(t) - \mathbf{F}^{\mathrm{int}}(t) \ , \tag{13}$$

$$\mathbf{P}_{\mathrm{int}}(\mathbf{d}(t),\ \mathbf{\Phi}(t)) = \mathbf{P}_{\mathrm{ext}}(t) \ . \tag{14}$$

Here $\mathbf{M}$ is the mass matrix which we take as lumped, $\mathbf{d}$ the vector of nodal mechanical displacements, $\mathbf{\Phi}$ the vector of nodal electric potential, $\mathbf{F}^{\mathrm{ext}}$ and $\mathbf{F}^{\mathrm{int}}$ are vectors of nodal forces equivalent to externally applied surface tractions and internal stresses respectively, $\mathbf{P}_{\mathrm{int}}$ is the nodal charge vector equivalent to internal polarization in piezoelectric elements, and $\mathbf{P}_{\mathrm{ext}}$ is the externally applied nodal charge vector.

Equation (13) is solved by the central-difference method. For linear problems, this technique and the lumped mass matrix yield exact time periods for the waves; it is hoped that the error, if any, in the time period for nonlinear waves will be small. Thus knowing the nodal mechanical displacements at time t_n, their values at time $t = t_{n+1}$ are given by

$$\mathbf{d}(t_{n+1}) = \Delta t_2\mathbf{M}^{-1}\left[(\mathbf{F}^{\mathrm{ext}}(t_{n+1}) - \mathbf{F}^{\mathrm{int}}(t_{n+1}))\frac{\Delta t_1+\Delta t_2}{2} + \left(\frac{1}{\Delta t_1}+\frac{1}{\Delta t_2}\right)\mathbf{d}(t_n) + \frac{\mathbf{d}(t_{n-1})}{\Delta t_1}\right] \tag{15}$$

where $\Delta t_1 = t_n - t_{n-1}$, $\Delta t_2 = t_{n+1} - t_n$. Recalling that the central-difference method with the lumped mass matrix is explicit and conditionally stable, we take

$$\Delta t = 1.8/\omega_{\max} \tag{16}$$

where $\omega_{\max}$ is the maximum frequency of free vibration of the discretized structure. Of course, essential boundary conditions must be enforced when solving Eqs. (13) or (15). Because the problem being studied is nonlinear, $\omega_{\max}$ needs to be computed after every time step.

We use the Newton-Raphson iterative method to solve Eq. (14) and write it in the incremental form as

$$\mathrm{J}(\mathbf{\Phi}(t_n),\ \mathbf{d}(t_{n+1}))\Delta\mathbf{\Phi}^{(i)}_{n+1} = -\mathbf{P}_{\mathrm{int}}(\mathbf{\Phi}^{(i-1)}(t_{n+1}),\ \mathbf{d}(t_{n+1})) + \mathbf{P}_{\mathrm{ext}}(t_{n+1}) \ , \tag{17}$$

where

$$J(\mathbf{\Phi}(t_n),\ \mathbf{d}(t_{n+1})) = \left.\frac{\partial\mathbf{P}_{\mathrm{int}}}{\partial\mathbf{\Phi}}\right|_{(\mathbf{\Phi}(t_n),\,\mathbf{d}(t_{n+1}))} \ ,$$
$$\mathbf{\Phi}^{(i)}(t_{n+1}) = \mathbf{\Phi}^{(i-1)}(t_{n+1}) + \Delta\mathbf{\Phi}^{(i)}(t_{n+1}) \ , \tag{18}$$
$$\mathbf{\Phi}^{(0)}(t_{n+1}) = \mathbf{\Phi}(t_n) \ .$$

The iterative process is stopped when

$$\|\Delta\mathbf{\Phi}^{(i)}(t_{n+1})\| / \|\mathbf{\Phi}^{(i)}(t_{n+1})\| \le \epsilon \ , \tag{19}$$

ϵ being a preassigned small number; it was set equal to 10^{-5} for results presented below.

For a smart structure, the number of nodal mechanical displacements far exceeds the number of nodal electrical potentials and the aforementioned explicit/implicit technique of analysing the problem is computationally very effective.

4
Computation and discussion of results

4.1
Validation of the code

A finite element code based on the formulation given above has been developed and debugged. It was validated first by solving a dynamic problem for a clamped-clamped square graphite/epoxy plate modeled as a linear elastic orthotropic lamina. The response of the plate subjected to a suddenly applied point load at its center computed with the present code matched very well with that computed with ABAQUS. We note that ABAQUS first computes the eigenmodes and thus decouples the mechanical degrees of freedom. For the quarter of the 200 mm × 200 mm × 1 mm plate divided into $10\times10\times1$ elements, we considered the first 100 eigenmodes to compute the solution with ABAQUS.

For the second test problem, we assumed the following displacement fields:

$$\text{Case 1}: \; u_1 = 20X_L X_L \sin\Omega t, \quad u_2 = 0, \quad u_3 = 0;$$
$$\text{Case 2}: \; u_1 = 0, \quad u_2 = 20X_L X_L \sin\Omega t, \quad u_3 = 0; \quad (20)$$
$$\text{Case 3}: \; u_1 = u_2 = 0, \quad u_3 = 10^5 X_2^2 X_3^2 \sin\Omega t \;,$$

with $\Omega = 1.257 \times 10^6/\text{s}$. For an orthotropic neo-Hookean plate, we computed the body force required to satisfy the balance of linear momentum (1), the initial velocity field, and displacements at the edges of the plate. The developed code was used to analyse the problem with these initial and boundary conditions and body forces. In each case, the computed solution was found to match well with the corresponding analytical solution of the problem.

A third test problem analysed was an 80 mm × 8 mm × 0.5 mm graphite/epoxy cantilever lamina with an 8 mm × 8 mm × 0.5 mm piezoelectric (PZT) actuator affixed, with its left edge 40 mm from the clamped edge, to its top surface. Both materials were modeled as linear elastic with the lamina as orthotropic and the PZT as transversely isotropic; values of material parameters given in Batra et al. (1996) were used. A point load was applied at each corner of the free end; the load increased linearly from 0 to 1N in 200 μs, was maintained at 1N for 100 μs and then decreased linearly to 0 in 200 μs. The time histories of the transverse displacement of the point of application of the point load and the voltage output at the top right corner of the PZT patch as computed by ABAQUS (Version 5.2) and the present code are plotted in Fig. 1; it is clear that the two results agree well. We note that problems involving nonlinear response of PZTs can not be analysed with ABAQUS.

Crawley and Anderson (1990) applied large driving voltages that increased linearly with time to the two sides of an unconstrained 20 mm × 10 mm × 0.25 mm PZT-G1195 plate and found its response to be highly nonlinear. Tiersten (1993) modeled the experiment as a plane-stress problem and used a theory linear in displacement gradients but cubic in the driving electric field. He determined the material constants for the PZT by the least squares method and found that the computed response matched very well with the observed one. Here we simulate Crawley and Anderson's experiment by using our code. The edges of the unconstrained PZT plate are taken to be stress free, and points on the bottom surface are constrained from moving in the thickness direction. A uniform voltage increasing linearly at 100 V/μs is applied to the top surface with the bottom surface grounded. Because of the symmetry of the problem about the two centroidal axes, only a quarter of the plate is modeled by a 20 × 10 × 2 uniform mesh. To study the small deformation/large electric field problem, it is reasonable to model the PZT by the following constitutive relation, obtained from (5) and (6) by retaining terms, linear in $\mathbf{E}$ but quadratic in $\mathbf{W}$

$$\begin{aligned}
\overline{\mathbf{T}} &= (2c_1 I_1 + c_3 I_2 + e_1 I_3 + v_2 I_3^2 + v_7 II_3)\mathbf{a}\otimes\mathbf{a} \\
&\quad + (2c_2 I_2 + c_3 I_1 + e_2 I_3 + v_4 I_3^2 + v_8 II_3)\mathbf{1} \\
&\quad + c_4(\mathbf{a}\otimes\mathbf{E}\cdot\mathbf{a} + \mathbf{a}\cdot\mathbf{E}\otimes\mathbf{a}) + 2c_5\mathbf{E} \\
&\quad + (e_3 + v_{11} I_3)(\mathbf{a}\otimes\mathbf{W} + \mathbf{W}\otimes\mathbf{a}) + v_{12}\mathbf{W}\otimes\mathbf{W}, \\
-\mathbf{P} &= (2\epsilon_1 I_3 + e_1 I_1 + e_2 I_2 + \mu_2 II_3 + 2v_2 I_1 I_3 \\
&\quad + 2v_4 I_2 I_3 + v_{11} II_4)\mathbf{a} \\
&\quad + 2(\epsilon_2 + \mu_2 I_3 + v_7 I_1 + v_8 I_2)\mathbf{W} \\
&\quad + 2(e_3 + v_{11} I_3)\mathbf{E}\cdot\mathbf{a} + 2v_{12}\mathbf{E}\cdot\mathbf{W} \;. \qquad (21)
\end{aligned}$$

We assigned following values to material parameters (see Tiersten 1993).

$$\begin{aligned}
&c_1 = 29 \text{ GPa}, \quad c_2 = 38.1 \text{ GPa}, \quad c_3 = -2 \text{ GPa} \;, \\
&c_4 = -21 \text{ GPa}, \quad c_5 = 35.9 \text{ GPa} \;, \\
&e_1 = 13.4757\,\text{C/m}^2, \quad e_2 = -39.8583\,\text{C/m}^2 \;, \\
&e_3 = 0, \quad \rho = 7,500 \text{ kg/m}^3 \;, \\
&v_4 = -90.3 \times 10^{-6} \text{ Pa m}^2/\text{V}^2 \;, \\
&v_{12} = 30.54 \times 10^{-6} \text{ Pa m}^2/\text{V}^2 \;, \\
&\epsilon_0 = 8.8419 \times 10^{-12} \text{ N/V}^2 \;, \\
&\epsilon_1 = 1.081 \times 10^{-9} \text{ N/V}^2 \;, \\
&\epsilon_2 = -2.22558 \times -10^{-9} \text{ N/V}^2 \;. \qquad (22)
\end{aligned}$$

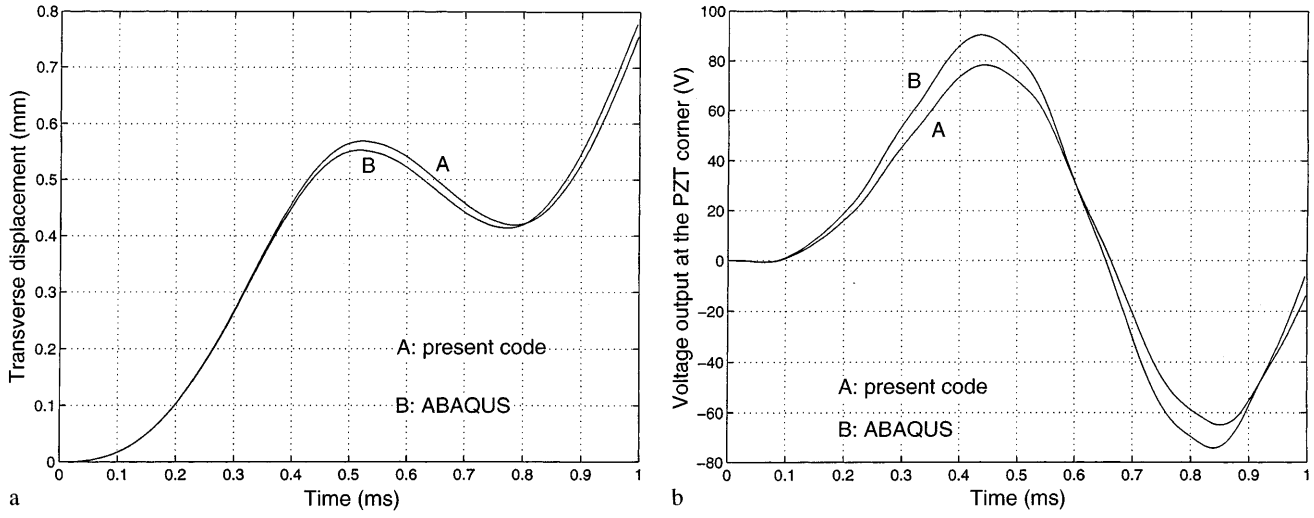

Fig. 1a, b. A comparison of the time histories, as computed by ABAQUS and the present code, of **a** the transverse displacement under the point load applied to a composite plate, and **b** the voltage output at the top right corner of the PZT patch

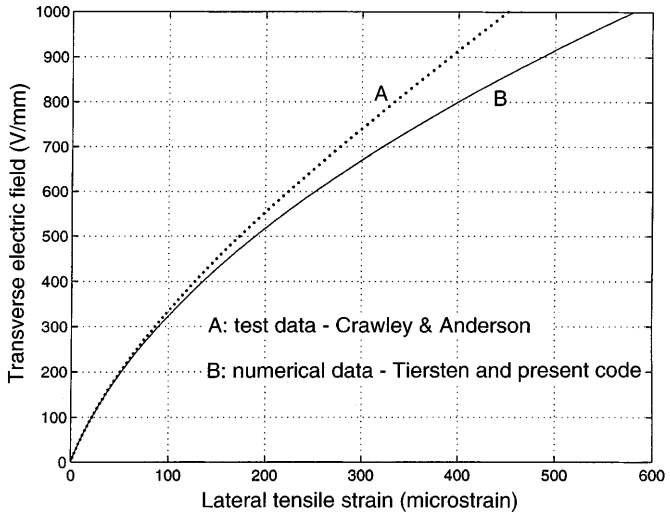

Fig. 2. A comparison of Crawley and Anderson's test data and Tiersten's results of the lateral tensile strain at the centroid of the PZT-plate vs. the transverse electric field with that computed by using the present code

The computed variation at the PZT centroid of the lateral tensile strain with the transverse electric field is compared in Fig. 2 with the test results and also with that given by Tiersten. It is clear that our result is in close agreement with Tiersten's analytical result, and in good agreement with Crawley and Anderson's experimental result. Tiersten incorporated a third-order term in the electric field, and obtained results very close to the test values.

4.2
Flexural waves in a cantilever beam

We now simulate experiments of Moetakef et al. (1996) on wave propagation in a beam and delineate the effects of the nonlinear response of PZTs. Their experimental set up, consists of a 1500 mm $\times$ 25.4 mm $\times$ 3.175 mm cantilever 6061-T65 aluminum beam with two 25.4 mm $\times$ 25.4 mm $\times$ 1.3716 mm PZT-850 patches bonded to its upper and lower surfaces abutting the free edge. A single sinusoidal pulse of 250 V amplitude and 500 μs time period is applied to the PZT surfaces. The transverse velocity at six points A through F on the top surface of the beam was measured by a fiber optic interferometer. With the origin of the rectangular Cartesian coordinate system at the centroid of the free end, x_3-axis pointing upwards and x_1-axis into the beam (cf. Fig. 3), coordinates (in mm) of points A through F are (0, 12.7, 2.9591), (6.35, 12.7, 2.9591), (19.05, 12.7, 2.9591), (101.6, 12.7 1.5875), (152.4, 12.7, 1.5875), (203.2, 12.7, 1.5875). Thus points A, B and C are on the longitudinal edge of the top surface of the PZT patch, and D, E and F are on the longitudinal edge of the top surface of the aluminum beam. Due to the symmetry about the x_1-x_3 plane, only one-half of the structure is modeled. Since the generated disturbance is a plane wave perpendicular to the direction of propagation, one element in the x_2-direction should suffice. In the region with $x_1 < 476.25$ mm, wherein points A through F are located, a fine mesh with element size (in mm) $1.5875 \times 1.5875 \times 0.79375$ is used; elsewhere the element size equals $3.175 \times 1.5875 \times 0.79375$. The element size in the PZT actuators (in mm) is $1.5875 \times 1.5875 \times 0.6858$. The values of material constants for the PZT-850 are taken to be the same as those for the PZT-2 (the two are equivalent according to the American Piezoceramics Inc.). These and material parameters for aluminum modeled as an isotropic material are listed below.

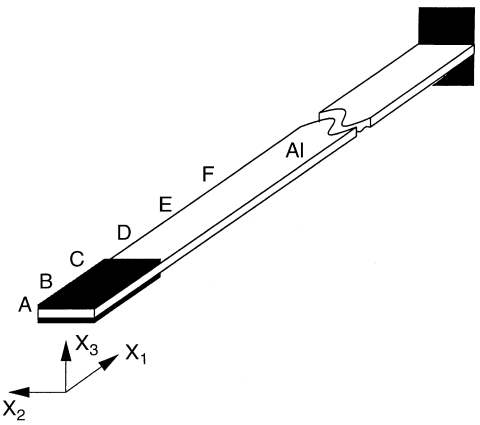

Fig. 3. A sketch of the setup of Moetakef et al.'s experiment on wave propagation in a cantilever aluminum beam (not to scale)

Piezoelectric material:

$$c_1 = 23.1 \text{ GPa}, \quad c_2 = 33.944 \text{ GPa}, \quad c_3 = 199.6 \text{ MPa},$$
$$c_4 = -22.535 \text{ GPa}, \quad c_5 = 33.49 \text{ GPa},$$
$$e_1 = 8.67544 \text{ C/m}^2, \quad e_2 = 1.85657 \text{ C/m}^2,$$
$$e_3 = -9.77768 \text{ C/m}^2,$$
$$\epsilon_0 = 8.8419 \times 10^{-12} \text{ N/V}^2,$$
$$\epsilon_1 = 1.08 \times 10^{-9} \text{ N/V}^2, \quad \epsilon_2 = -2.22558 \times 10^{-9} \text{ N/V}^2,$$
$$\rho = 7,600 \text{ kg/m}^3 \tag{23}$$

Aluminum:

$\rho = 2,700$ kg/m^3, Young's modulus $= 68.965$ GPa, Poisson's ratio $= 0.3269$.

Time histories of the transverse velocity of points A, C and E, as computed by the present code using the infinitesimal theory, observed experimentally, and computed by Moetakef et al. (1996) by the finite element method are plotted in Figs. 4a through 4c; Moetakef et al. used tetrahedral elements, modeled a quarter of the structure, and employed a Newmark-Wilson time integration scheme; their finite element mesh had one element in the thickness direction in the PZT and in the aluminum beam. Results for other three points are given in Liang (1997). The two sets of computed results agree well for points A, B and C on the top PZT patch. However, they differ noticeably from the test values at points A and B. At point C, our computed results are in better agreement with the observed values than those of Moetakef et al. For points D and E on the aluminum beam, our computed results are closer to the experimental results than those of Moetakef et al., and for point F, the two sets of computed results differ noticeably from the test data. Except for points A and F, the finite element results at other points are in good agreement with those observed experimentally. Moetakef et al. noted that the agreement between the computed and

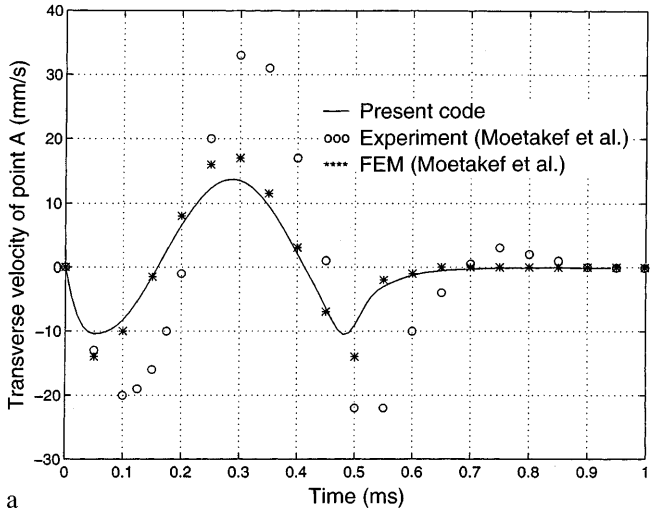

a

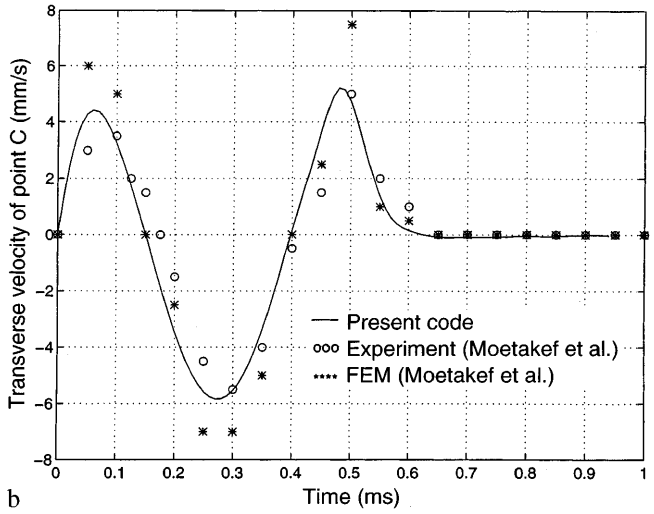

b

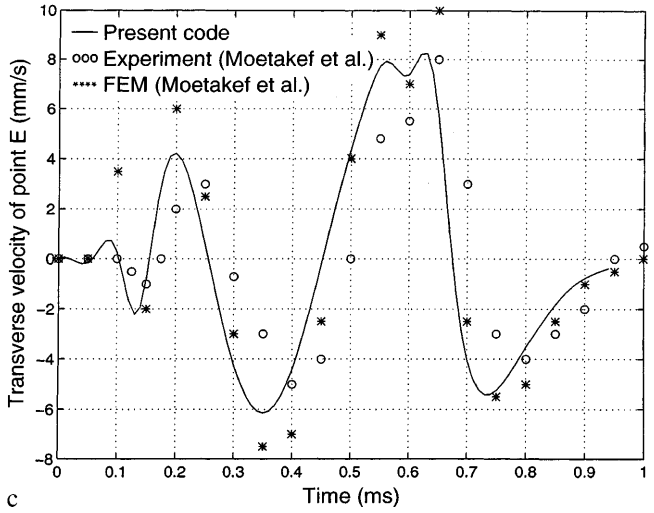

c

Fig. 4a–c. A comparison of the test data of Moetakef et al. and their computed results of the time histories of the transverse velocities of points A, C and E on a cantilever beam actuated by two PZT patches bonded near its free edge with the corresponding results computed by using the present code

observed values of the transverse velocity at points A through F was not improved by using a finer finite element mesh. Factors for the difference between the computed and experimental results include the higher stiffness of the discrete model, neglecting in the *FE* model the effect of the adhesive layer between the PZT patch and the aluminum beam, differences between the values of material constants for the PZT-850 and the PZT-2, ignoring hysteresis in the PZT, collecting every eighth data point in the experiment, smoothening of the test data, and the generated wave being not a plane wave.

We now model the aluminum as an isotropic neo-Hookean material, and the PZT as a transversely isotropic neo-Hookean material. For results presented in Fig. 4, only terms linear in $\mathbf{W}$ are retained in (21). Time histories of the axial and lateral strains and the axial and lateral normal stresses at four points, P, Q, R and S on the vertical line through the point (6.685 mm, 0.335 mm, 0) are exhibited in Fig. 5; time histories of the other components of strain and stress are omitted for brevity. Note that points P and Q are in the beam, and R and S are in the PZT patch. The inplane shear strain E_{12} was found to be two orders of magnitude smaller than the axial strain, and the transverse shear strains and the transverse normal strain an order of magnitude smaller than the axial strain. However, the normal strains in the x_1- and x_2-directions are of the same order of magnitude, and are in phase with each other; E_{33} was found to be 180° out of phase with E_{11}. Each curve is a sine wave of 500 μs duration implying that a sinusoidal impulse generates sinusoidal strains and stresses. We recall that the vertical line under consideration passes through the PZT patch and the computed results indicate that the axial and lateral normal stresses at points R and S in the PZT patch are compressive but those at points P and Q are tensile. Thus the distribution of the axial stress on a vertical line passing through points P, Q, R and S in the portion of the aluminum beam with the PZT patches is quite different from that on a vertical line in a monolithic beam.

In Eq. (21) terms multiplying v_2, v_4 and v_{12} are quadratic in $\mathbf{W}$. With the PZT poled in the x_3-direction and the voltage difference also applied in the x_3-direction, terms multiplying v_2 and v_{12} can be added together, or equivalently only one of them can be considered. Since values of v_4 and v_{12} for PZT-850 are unknown, we assume that they are in the same range as those for PZT-G1195 tested by Crawley and Anderson (1990) and examined above. Figures 6a–6d depict, for three different values of v_4, with $v_{12} = 0$, the time-history of the transverse velocity and displacement of point B, and of the axial strain and stress at the point (6.685, 0.335, 2.418) mm in the top PZT patch; results for other points are omitted. It was found that v_4 has a small effect on the transverse velocity and deflection of point A, and has no effect on the transverse velocity and displacement of points D, E, and F. However, v_4 affects noticeably the transverse velocity and displacement of points B and C. As for results computed with the

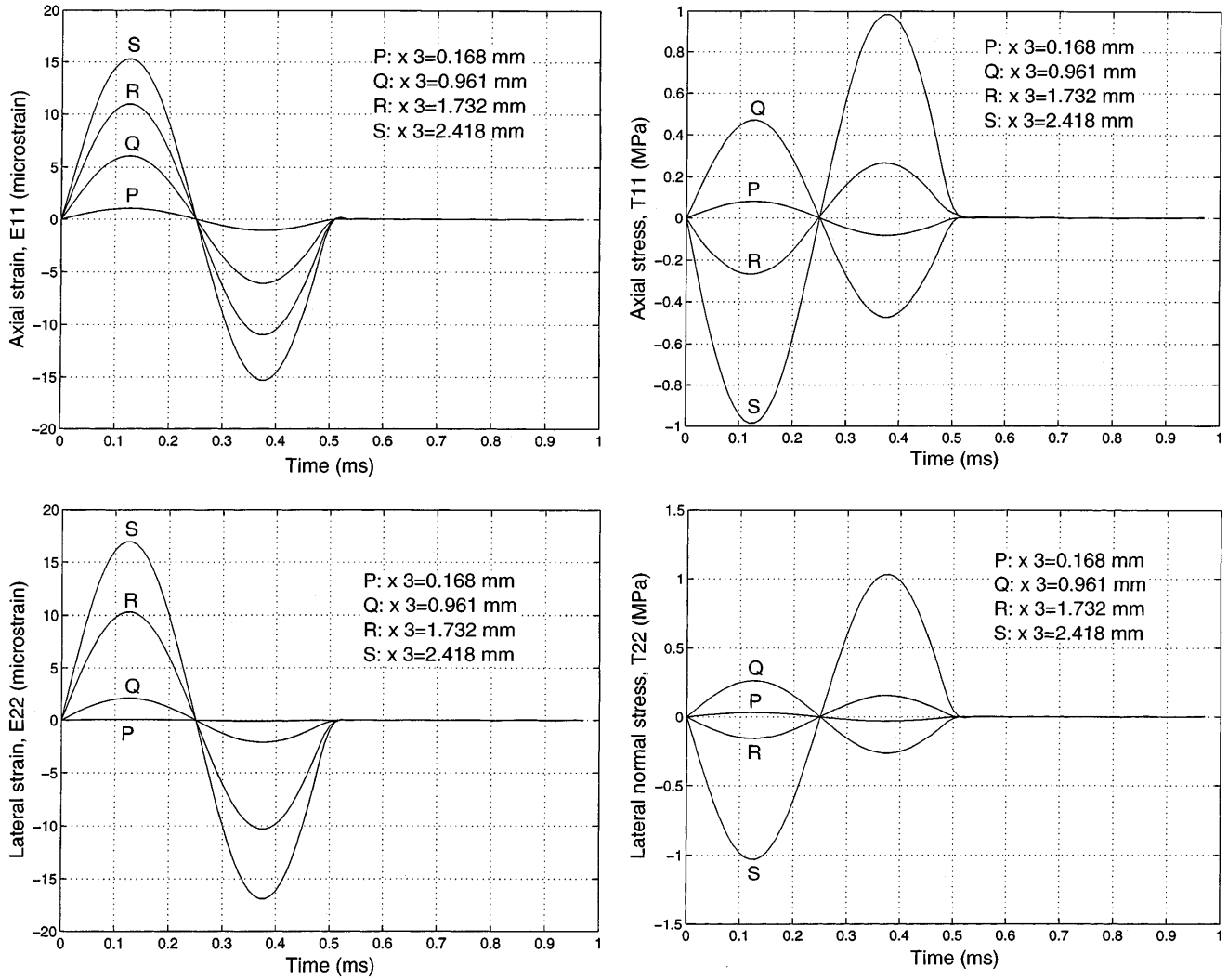

Fig. 5. Time histories of the axial and lateral strains, and axial and lateral stresses at four points on a vertical line in Moetakef et al.'s experiment on flexural vibrations of a beam

linear theory, axial stress and axial strain at the point (6.685, 0.335, 2.418) mm in the PZT are nearly 180° out of phase with each other. Also E_{22} and T_{22} were found to be about 180° out of phase with each other but the remaining components of stress were in phase with the corresponding components of strain. The overall agreement between the computed and observed transverse velocities at the six points A through F, described above, is not greatly improved by considering the term with v_4. We notice, however, that the agreement between the computed and observed velocities at point B is better for $v_4 = -1 \times 10^{-4}$ Pa m^2/V^2 than that for $v_4 = 0$. Figures 7a through 7d depict, for three different values of v_{12}, with $v_4 = 0$, the time histories of the transverse velocity and displacement of point B, and of the axial strain and stress at the point (6.685, 0.335, 2.418) mm in the top PZT patch; results for other points are omitted. As was the case for v_4, v_{12} has a small effect on the transverse velocity and displacement of point A, has essentially no effect on the transverse velocity and displacement of points D, E and F, but has noticeable effect on transverse velocity and displacements of at points B and C.

Every component of strain and stress tensors at the point (6.685, 0.335, 2.418) mm in the top PZT is significantly influenced by v_4 and v_{12}. The longitudinal strain and stress are no longer a sinusoidal function of time for the PZTs with nonzero values of v_4 and/or v_{12}. Also, the magnitude of T_{11} is higher for the PZT with nonzero v_4 and/or v_{12} as compared to that for $v_4 = v_{12} = 0$. The response for the positive applied voltage is quite different from that for the negative applied voltage.

4.3
Flexural waves in a defective cantilever beam

In an attempt to see if the propagation of flexural waves in a cantilever beam can be used to delineate a defect in it, we use Moetakef et al.'s (1996) set up discussed above but introduce a 9.525 mm × 1.5875 mm × 1.5875 mm weak region located at 184.15 mm from the free edge; one surface of the weak region abuts the midsurface of the beam. The elastic constants for the material in the weak region equalled 10^{-5} of those in the remainder of the beam. Figures 8 and 9 depict the time histories of the transverse velocity and the voltage output from the PZT sensor

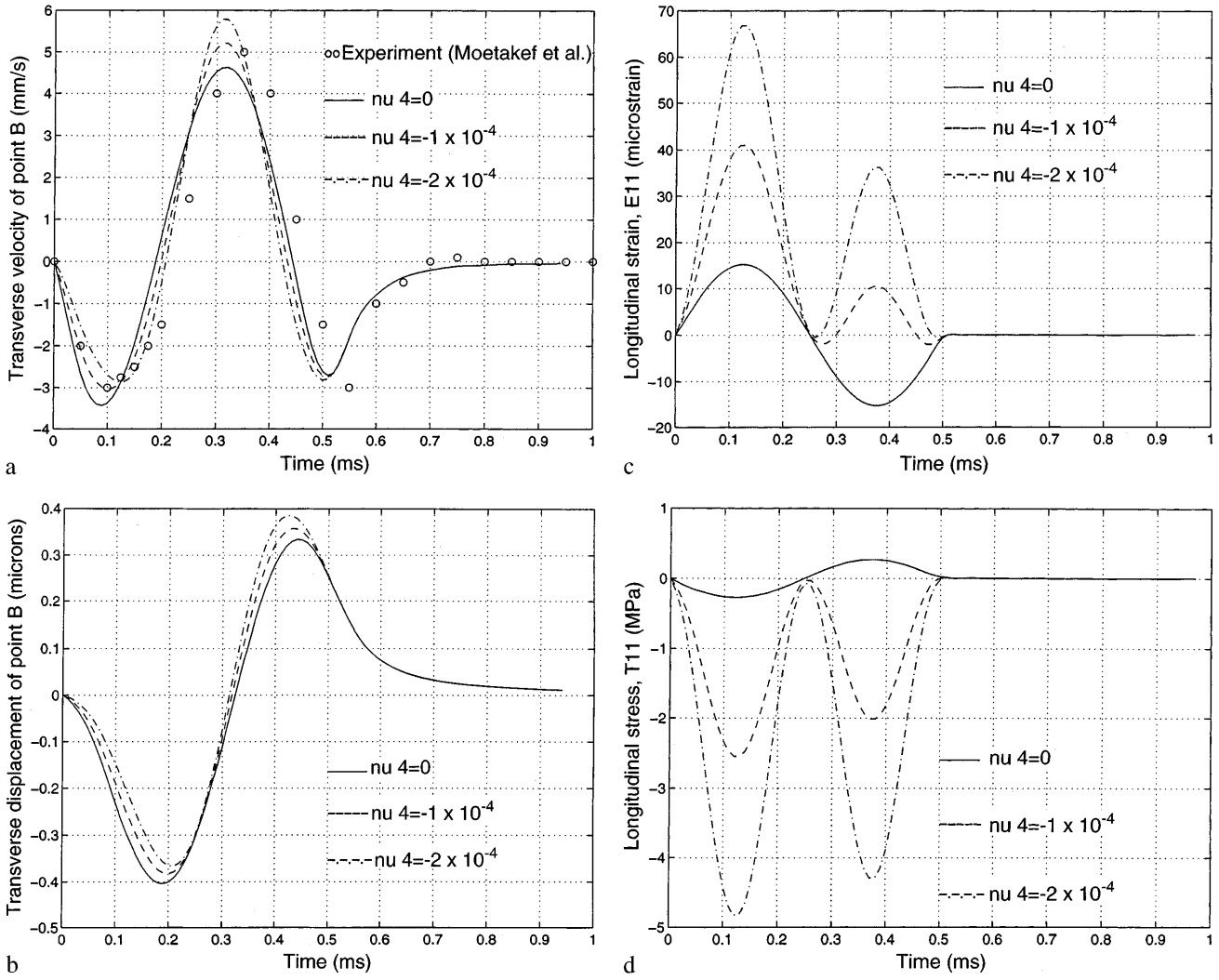

Fig. 6a–d. Time histories of the transverse velocity and displacement of point B, and of the axial strain and stress at the point (7.02, 9.36, 2.418) mm in the PZT for three different values of v_4 with $v_{12} = 0$

bonded to the upper surface of the beam at a distance of 233.36 mm from the free edge. The results exhibited are for a neoHookean beam, but similar results were obtained for a linear elastic beam. The differences in the time-histories of the transverse velocities for beams with and without defects is not large enough for the technique to be of practical use.

4.4
Active control of a nonlinear cantilever plate

We now consider a three-layer (0/90/0) 60 mm × 40 mm ×3 mm graphite/epoxy cantilever plate with three 4 mm × 12 mm × 1mm PZT-G1195 sensors bonded to its top surface and three 4 mm × 8 mm × 1mm PZT-G1195 actuators affixed to its bottom surface as shown in Fig. 10. Each PZT patch is prepoled in the x_3-direction. The goal is to annul vibrations of the plate when a sinusoidal impact force of amplitude 20 N and time period 2 ms is applied for 1 ms at each node on the free edge.

In order to actively control the structure, each sensor is connected to a corresponding actuator to form a closed-loop system. A simple constant-gain position feedback control algorithm (Ha et al. 1992) is employed. The ith sensor output is multiplied by a gainfactor, G_i, and the resulting voltage is uniformly applied to the ith actuator. Generally, the voltage induced in a sensor does not affect much its mechanical response through the converse piezoelectric effect. Hence we presume that the dynamic output from a sensor is due to its mechanical deformations only. We assume that the gain factor, $G_i = 10^7$ V/m, is the same for each sensor-actuator pair. The open-loop responses of the structure using both linear elastic and neo-Hookean material models were found to be virtually indistinguishable because of the infinitesimal strains induced. Results presented herein are for the neo-Hookean material and the response of the piezoelectric material represented by Eq. (21) with material parameters given by (24).

We focus on minimizing the vibrations of points A through F shown in Fig. 10, and accomplish this by using first the sets of sensors and actuators nearest to the fixed support, then by using this and also the adjoining sets, and finally all three sets. Figures 11a–11f depict the time histories of the transverse displacement of points $A-F$ for these three cases, and also for the uncontrolled case. It is

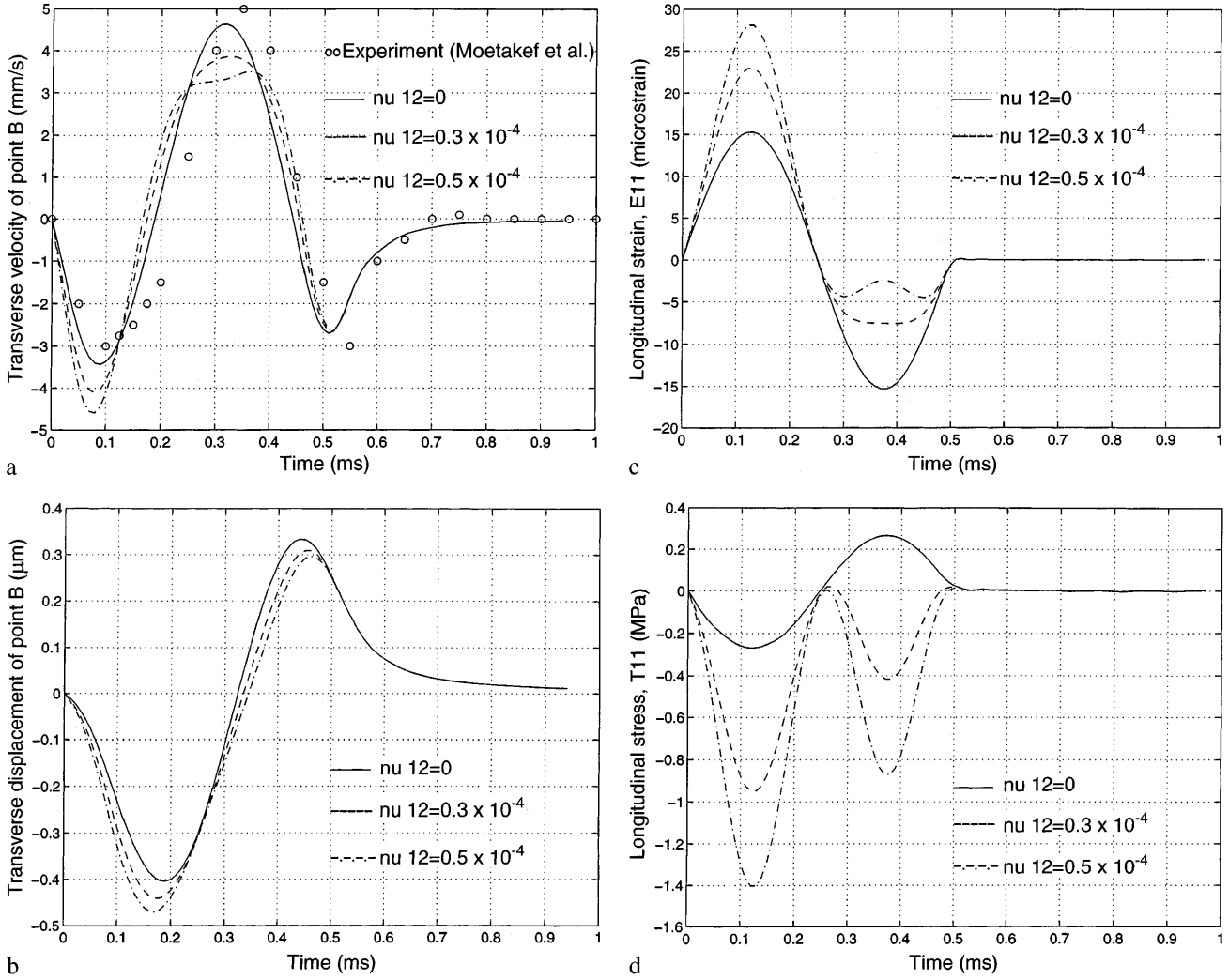

Fig. 7a–d. Time histories of the transverse velocity and displacement of point *B*, and of the axial strain and stress at the point (7.02, 9.36, 2.418) mm in the PZT for three different values of v_{12} and $v_4 = 0$

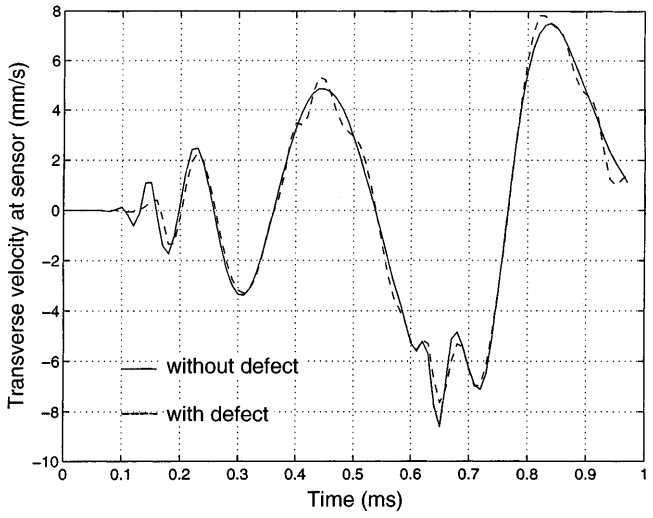

Fig. 8. Time history of the transverse velocity of a top right corner of the PZT sensor on the cantilever beam, used in Moetakef et al.'s experiment, with and without a defect in it.

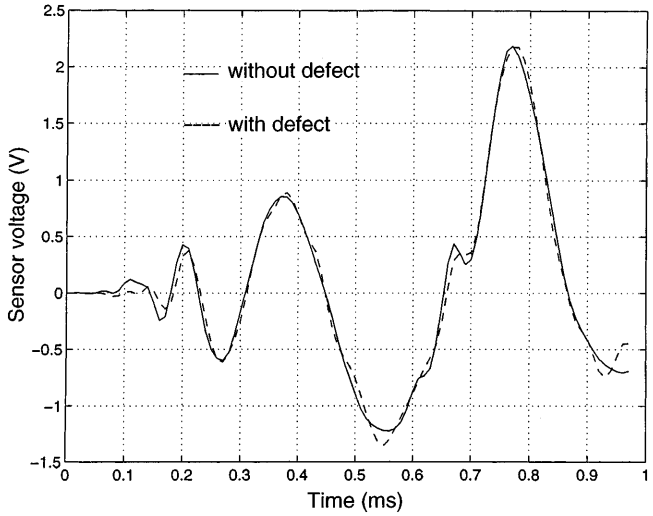

Fig. 9. Time history of the sensor voltage with and without a defect in the Moetakef et al.'s cantilever beam

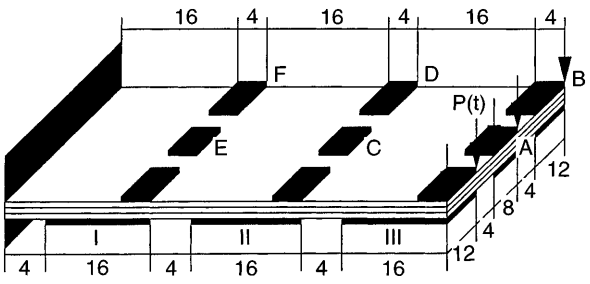

Fig. 10. A set up of the smart plate

Fig. 11 Time histories of the transverse displacements of points *A* through *F* when **a** no sensors and actuators **b** sensors and actuators in Column I closest to the fixed support, or **c** sensors and actuators in Columns I and II, or **d** all sensors and actuators are activated

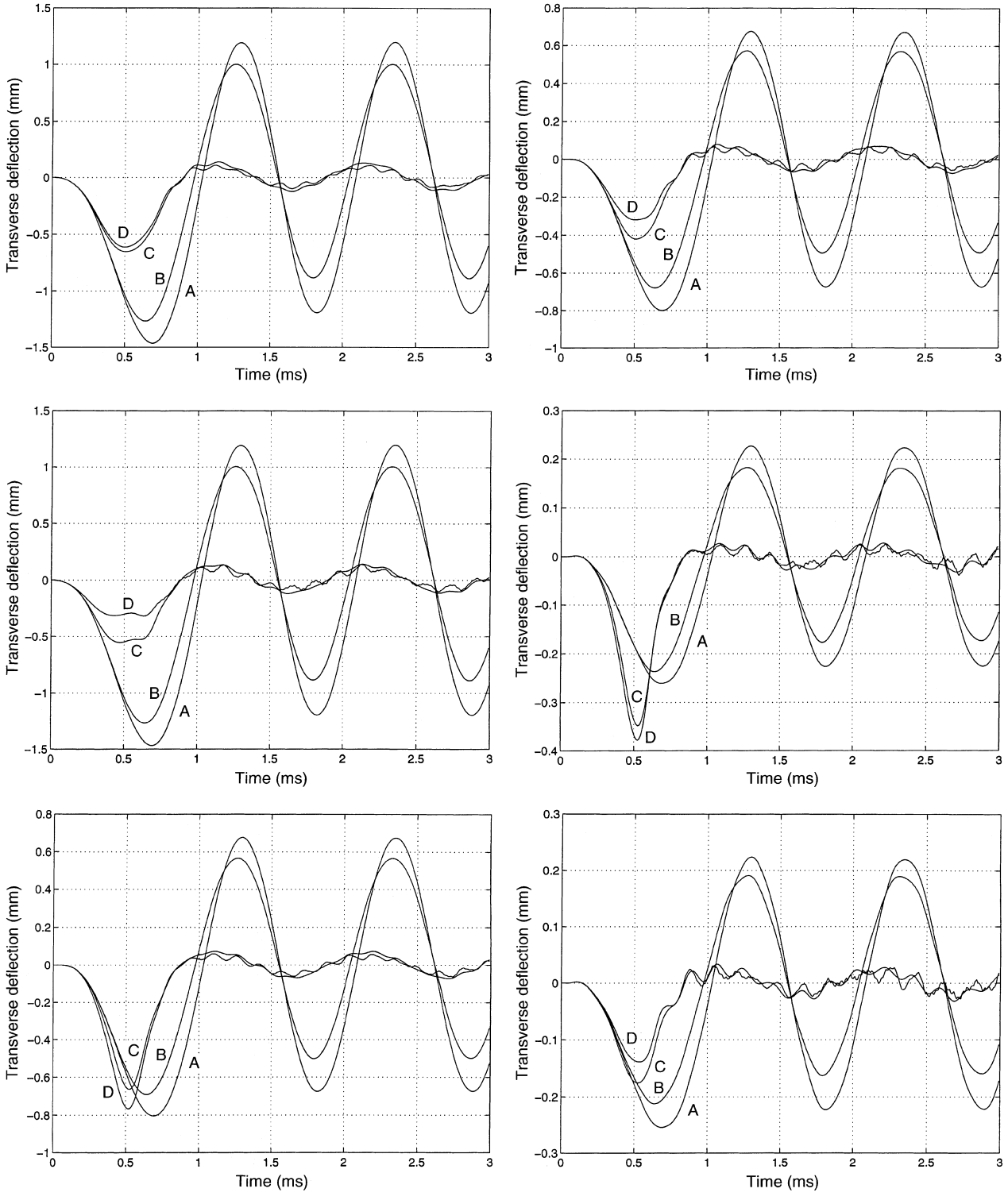

clear that the actuators placed near the free end are more effective in diminishing the vibrations of points $A-F$, and the sensor/actuator pair located closest to the fixed end of the plate slightly reduces the amplitude of vibrations of points $A-F$.

5 Conclusions

We have developed and validated a finite element code to analyse 3-dimensional transient deformations of a neo-Hookean body with piezoelectric patches either affixed to its bounding surfaces or embedded in it. The code has been used to analyse Crawley and Anderson's experiment on ascertaining the response of an unconstrained PZT plate to large driving voltages, and Moetakef et al.'s experiment on the propagation of flexural waves in a cantilever beam. In each case the computed and observed results are found to agree with each other within acceptable limits. The code is then used to study the propagation of flexural waves in a defective neoHookean cantilever beam, and the sensor output is found to be essentially insensitive to the defect considered. It is found that a simple feedback control algorithm in which the actuator input voltage is proportional to the transverse displacement of the sensor effectively annuls the vibrations of a neoHookean cantilever plate subjected to an impulsive load.

References

Allik, H.; Hughes, T. J. R. (1970): Finite element method for piezoelectric vibration. Int J Num Meth Eng 2, 151–157

Batra R. C.; Ghosh, K. (1995): Deflection control during dynamic deformations of a rectangular plate using piezoceramic elements. AIAA J 33, 1547–1549

Batra, R. C.; Liang, X. Q. (1996): Shape control of vibrating simply supported rectangular plates. AIAA J 34, 116–122

Brooks, S.; Heyliger, P. (1994): Static behavior of piezoelectric laminates with distributed and patched actuators. J Intell Mat Struct 5, 635–646

Chandrashekhara, K.; Agarwal, A. N. (1993): Active vibration control of laminated composite plates using piezoelectric devices: A finite element approach. J Intell Mat Syst Struct 4, 496–508

Crawley, E. F.; Anderson, E. H. (1990): Detailed models of piezoceramic actuation of beams. J Intell Mat Struct 1, 4–24

Dosch, J.; Leo, D.; Inman, D. J. (1993): Modeling and control for vibration suppression of a flexible smart structure. In: Kirk, C. H.; Hughes, P. C. (eds) Dynamics and control of Structures in Space II, Comput Mech Publ 603–618

Fuller, C. R.; Hanson, C. H.; Snyder, S. D. (1991): Active control of sound radiation from a vibrating rectangular panel by sound source and vibration inputs, an experimental comparison. J Sound Vibr 145, 195–215

Ha, S. K.; Keilers, C.; Chang, F. K. (1992): Finite element analysis of composite structures containing piezoceramic sensors and actuators. AIAA J 30, 772–780

Hall, E. K. II; Muller, J. T. (1995): Coupled vibration isolation/suppression system for space applications. In: Chopra, I. (ed.) Aspects of structural design SPIE 2443, 136–144

Hanagud, S.; Obal, M. W.; Calise, A. J. (1987): Optimal vibration control by the use of piezoceramic sensors and actuators. Proc. AIAA/ASME/AHS/ASEE 28th Structures, Structural Dynamics, and Materials Conference, Paper #87-0959, Monterey, CA, April 6–8

Hauch, R. M. (1995): An industrial approach to static and dynamic finite element modeling of composite structures with embedded actuators. Chopra, I. (ed.) Smart Structures and Integrated Systems. SPIE 2443, 458–469

Heeg, J.; McGowan, A.; Crawley, E.; Lin, C. (1995): The piezoelectric aeroelastic response tailoring investigation: A status report. In: Industrial and Commercial Applications of Smart Structures Technologies, SPIE 2447, 2–12

Huang, Y. N.; Batra, R. C. (1996): A theory of thermoviscoelastic dielectrics. J Thermal Stress 19, 419–430

Hughes, T. J. R. (1987): The finite element method, linear static and dynamic finite element analysis. Prentice-Hall, Englewood, NJ

Im, S.; Atluri, S. N. (1989): Effects of a piezo-actuator on a finitely deformed beam subjected to general loading. AIAA J 27, 1801–1807

Johnson, M. E.; Elliott, S. J. (1995): Experiments on the active control of sound radiation using a volume velocity sensor. In: Chopra, I. (ed.) Smart Structures and Integrated Systems, SPIE 2443, 658–669

Kulkarni, G.; Hanagud, S. (1991): Modeling issue in the vibration control with piezo-ceramic actuators. In: Haritos, G. K.; Srinivasan, A. V. (eds.) Smart Structures and Materials, ASME, AD-24/AMD-123, 7–45

Lagoudas, D. C.; Bo, Z. (1994): The cylindrical bending of composite plates with piezoelectric and SMA layers. Smart Mat Struct 3, 309–317

Liang, X. Q. (1997): Dynamic response of linear/nonlinear smart structures. Doctoral Dissertation, Virginia Polytechnic Institute and State University, Blacksburg, VA

Maugin, G. A.; Pouget, J.; Drouot, R.; Collect, B. (1992): Nonlinear electromechanical coupling. John Wiley & Sons

Mollenhauer, D. H.; Griffin, O. H. Jr. (1994): Induced strain of actuation of surface bonded piezoceramic patches: A numerical and experimental study. J Intell Mat Syst Struct 5, 355–362

Norwood, D. S.; Shuart, M. J.; Herakovich, C. T. (1991): Geometrically nonlinear analysis of interlaminar stress in unsymmetrically laminated plates subjected to inplane mechanical loading. Proc. AIAA/ASME/ASCE/AHS/ACS 32nd Structures, Structural Dynamics and Material Conference, AIAA, Washington, DC. 938–955

Price, J. G.; Napoletano, F. M. (1995): Reducing interior acoustic field in vibrating cylinders. In: Chopra, I. (ed) Smart Structures and Integrated Systems SPIE 2443, 682–691

Qiu, J. H.; Tani, J. (1996): Vibration suppression of a cylindrical shell using a hybrid control method. J Intell Mat Syst Struct 7, 278–287

Ray, M. C. H.; Rao, K. M.; Samanta, B. (1993): Exact solution for static analysis of an intelligent structure under cylindrical bending. Comput Struct 47, 1031–1042

Samanta, B.; Ray, M. C.; Bhattacharyya, R. (1996): Finite element model for active control of intelligent structures. AIAA J 34, 1885–1892

Song, O.; Librescu, L.; Rogers, C. A. (1992): Application of adaptive technology to static aeroelastic control of wing structures. AIAA J 30, 2882–2889

Srinivas, S.; Rao, C. V. J.; Rao, A. K. (1970) An exact analysis of vibration of simply supported homogeneous and laminated thick rectangular plates. J Sound Vib 12, 257–269

Suleman, A.; Venkayya, V. B. (1995): A simple finite element formulation for a laminated composite plate with piezoelectric layers. J Intell Mat Syst Struct 6, 776–782

Tiersten, H. F. (1971): On the nonlinear equations of thermoelectroelasticity. Int J Eng Sci 9, 587–604

Tiersten, H. F. (1975): Nonlinear electroelastic equations cubic in small field variables. J Acoust Soc Am 57, 660–666

Tiersten, H. F. (1993): Electroelastic equations for electroded thin plates subjected to large driving voltages. J Appl Phys 74, 3389–3393

Tzou, H. S.; Gadre, M. (1989): Theoretical analysis of a multilayer thin shell coupled with piezoelectric shell actuators for distributed vibration controls. J Sound Vibr 132, 433–450

Tzou, H. S.; Tseng, C. I.; Bahrami H. (1994): A thin piezoelectric hexahedron finite element applied to design of smart continua. Fin El Analys Design 16, 27–42
Wittrick, W. H. (1987): Analytical, three-dimensional elasticity solutions to some plate problems, and some observations on Mindlin's plate theory. Int J Solids Struct 23, 441–464
Wojicik, G. L.; Vaughan, D. K.; Abboud, N.; Mould, J. Jr. (1993): Electromechanical modeling using explicit time-domain finite elements. Proc. of IEEE Ultrasonics Symposium 1107–1112
Won, C. C.; Sulla, J. L.; Sparks, D. W. Jr.; Belvin, W. K. (1994) Application of piezoelectric device to vibration suppression. J Guid Contr Dyn 17, 1333–1338
Yang, J. S.; Batra, R. C. (1995): A second order theory for piezoelectric materials. J Accoust Soc Am 97, 280–288
Zhou, Y. S.; Tiersten, H. F. (1994): Elastic analysis of laminated composite plates in cylindrical bending due to piezoelectric actuators. Smart Mat Struct 3, 225–265